Transient gain from N_2^+ in light filaments

Ladan Arissian,[1,2] Brian Kamer,[1] Ali Rastegari,[1] D. M. Villeneuve,[2,3] and Jean-Claude Diels[1]
[1]*Center for High Technology Materials, Albuquerque, New Mexico 87106, USA*
[2]*Department of Physics, University of Ottawa, Ottawa, K1N 6N5, Canada*
[3]*Joint Attosecond Science Laboratory, National Research Council of Canada, Ottawa, K1A 0R6, Canada*

(Received 31 January 2018; revised manuscript received 19 July 2018; published 27 November 2018)

We present our results on the emissions from N_2^+ pumped with ultrafast filaments using high-resolution pump probe. Our result shows the phase relation between transition lines at earlier delays. We show that the gain on transition lines extends beyond the time when coherence is lost.

DOI: 10.1103/PhysRevA.98.053438

I. INTRODUCTION

Nonlinear light propagation in the atmosphere is of great interest as it can export the high-intensity optical fields from the laboratory to the real world, with applications to remote sensing and atmospheric studies. Since no optomechanical device can control the properties of a beam propagating freely through the atmosphere, the understanding of light matter interaction is an essential tool to control radiation, intensity, and profile of the beam in space. Light filaments [1,2] contain confined regions of high intensity, which can trigger nonlinear interactions, leading to supercontinuum, terahertz generation, strong field ionization, and stimulated emission. The latter mechanism is of particular interest because it can lead to forward and backward air lasing [3]. In this context, the mechanism of stimulated emission of the molecular nitrogen ion itself is of particular interest. Various mechanisms for gain have been proposed; electron recollision [4], strong field ionization [5], superradiance [6], and strong field interaction with plasma [7] with gain observed in laser dressed states [8].

In this paper, optical gain between electronic transitions in the vibrational ground states of N_2^+ is analyzed with high spectral resolution. The time evolution of the plasma following a 795 nm pump is indirectly measured by analyzing the stimulated emission driven by an ultrashort delayed broadband seed around 400 nm. The transitions of interest (first negative band) are between the electronic states of $B^2\Sigma_g^+$ (upper state) and the $X^2\Sigma_g^+$ (lower state), both in the vibrational ground state ($v = 0$). The gain at the wavelengths corresponding to the transitions between the rotational levels is observed as a function of delay between the ionizing 800 nm pulse and the frequency doubled seed whose spectrum overlaps with the transitions. The delay-dependent gain reveals a signature of the rotational wave packet launched into the system by the ionizing 800 nm pulse. Lei *et. al* [9] concluded that inversion is established between the upper and lower state by comparing the amplitude of the wave packets in those states. Other authors [10,11] highlight the effect of the seed itself in creating stimulated Raman process in the medium and further modulation of the gain. Liu *et. al* [12] reported that the near-resonant coherent Raman process provides laserlike emission. As all these measurements are either performed in time or frequency, our representation and analysis of the data in both domains provide a complementary picture to the emission and gain process. In this work, by performing high-resolution spectroscopy of the gain versus time, we observe a well-defined phase relation between the transitions. The ultrafast probing of the emission between individual rovibrational states suggests that two processes of resonant stimulated Raman scattering and stimulated gain are working in parallel, resulting in an intricate emission spectrum that depends on the phase and population of the relevant states. The coherence waveform generated by phase locking of rovibrational states in upper and lower state combined with the population modulation in stimulated Raman scattering result in a transient gain.

The fluorescence emission of N_2^+ with a lifetime of 62 ns [13] has been observed for centuries in the aurora borealis. Given the vibrational quantum number v and the rotational quantum number J, the energy levels can be tabulated through:

$$E = \omega_e\left(v+\tfrac{1}{2}\right) - X_e\omega_e\left(v+\tfrac{1}{2}\right)^2 + Y_e\omega_e\left(v+\tfrac{1}{2}\right)^3 + B_v J(J+1) - D_e J^2(J+1)^2 + T_e. \quad (1)$$

The first three terms are vibrational, the fourth and fifth terms are rotational, and the last term is the energy level of the electronic state for $J = 0$ and $v = 0$. The subscripts v and e refer to vibration and equilibrium states. The values for selected levels are (in cm^{-1}) $v' = 0$, $T_e = 0$, $\omega_e = 2207.00$, $\omega_e X_e = 16.10$, $\omega_e Y_e = -0.040$, $\alpha_e = 0.01881$, $B_e = 1.93176$, $D_e = 6.1 \times 10^{-6}$ for the **X** state (ion ground state) and $T_e = 25461.4$, $\omega_e = 2419.84$, $v'' = 0$, $\omega_e X_e = 23.18$, $\omega_e Y_e = -0.537$, $\alpha_e = 0.024$, $B_e = 2.07456$, $D_e = 6.17 \times 10^{-6}$ for the **B** state [14]. B_v is calculated as $B_v = B_e - \alpha_e(v+\frac{1}{2})$. The selection rules for transitions between rotational states are $\Delta J = 0, \pm 1$. Since both electronic states under consideration are Σ states, $\Delta J = 0$ (**Q** branch) is forbidden. The transitions from **X** to **B** states proceed along two branches known as **P** (lower-energy) and **R** (higher-energy) branches. Historically the spectrum was taken for absorption spectroscopy and the final state is usually referred to as the state with higher energy, so $\Delta J = J_{\text{upper}} - J_{\text{lower}} = 1$ results in higher-energy photons and $\Delta J = -1$ in lower-energy ones.

A nonresonant ultrashort pulse excites the rotational states in neutral and ionized molecules, particularly when the pulse length is much shorter than the characteristic revival time of $1/(2Bc)$, where $B = B_\nu$ is the rotational constant for a particular vibrational state. Such an ultrashort pulse has a spectrum that spans the full bandwidth of rotational energies in neutral and ionic states. In nonadiabatic regime of molecular alignment with ultrashort pulses [15], the molecular response is too slow to follow the rapidly changing potential. The impulsive excitation imparts a fixed phase relation on the rotational states. All diatomic molecules (including those that are ionized by the high field), are given a torque, which, quantum mechanically, modifies the J distribution through Raman transitions with $\Delta J = \pm 2$. Since this Raman excitation proceeds via discretely spaced levels at a well-localized initial time, a wave packet is created [16]. The discrete frequencies separated by $4Bc$ will rephase at time intervals of $1/(2Bc)$, in analogy to the mode-locking process taking place in an ultrashort pulse laser, where equidistant modes are phased such that ultrashort pulses are generated at each cavity round trip. The restoration of wave packets at equal time intervals referred to as revivals [17] takes place as long as the phase coherence is maintained. The change of alignment induced by linearly polarized light can be simply monitored by $\langle \cos^2\theta(t)\rangle$, where θ is the angle between the molecular axis and the light polarization, and $\langle\ \rangle$ indicates an average over the ensemble of molecules. For a linearly polarized weak ultrashort probe pulse propagating through this medium the refractive index is a time-dependent quantity proportional to $\langle \cos^2\theta(t)\rangle$. The carrier frequency of the probe beam is shifted by the derivative of the phase proportional to $d/dt\langle \cos^2\theta(t)\rangle$ [18,19]. The time-dependent index of refraction results in a bandwidth change of the probe, and also divergence of the seed beam. Also, the time evolution of molecular alignment is monitored through the transient index of refraction, which causes a shift in the wavelength of the probe pulse [18,19].

II. EXPERIMENTAL SETUP

A train of 50 fs pulses (FWHM of intensity) at 1 kHz repetition rate, 1.3 mJ energy each, centered at 795 nm, is generated by a Ti:sapphire oscillator-regenerative amplifier (Coherent-Hidra). The beam is focused (N.A 0.01) into a meter-long cell filled with nitrogen. A seed pulse is created by frequency doubling a 10% split-off from the main beam. A dichroic mirror is used to overlap the 795 nm pump beam with its second harmonic. The 940 μJ pump and 40 nJ seed are focused into a nitrogen cell with pressures ranging from 100–760 Torr. The 795 nm beam ionizes the medium, while the second harmonic beam is used to seed the $\mathbf{X}\ (\nu = 0) \leftarrow \mathbf{B}\ (\nu = 0)$ transitions at 391 nm. The delay between seed and pump is stepped with 7 fs increments. At each step the spectrum of the $N_2{}^+$ emission is measured over a 4 nm bandwidth with a resolution of 0.2 cm^{-1}. The intensities at the focus for those pulses, considering only linear focusing, are 5×10^{15} watt/cm^2 for the pump and 6×10^{11} watt/cm^2 for the seed pulse. Nonlinear focusing and defocusing of the light propagating in air limits the intensity of the 795 nm pump pulse in the range of 5×10^{13} to 10^{14} W/cm^2 [20].

The polarization of each beam is controlled with appropriate wave plates. In this study pump and seed are linearly polarized with parallel polarization. The pump and amplified seed are separated by a dichroic mirror two meters away from the focus. The 400 nm beam is further divided by an unpolarized beam splitter (96/4) and sent to two separate spectrometers. The smaller fraction goes to a large bandwidth and low-resolution instrument (Ocean Optics HR2000) to monitor the seed fluctuations and modulations; the major portion of the transmitted blue is focused onto the entrance slit of a high-resolution spectrometer. The latter is a 1.6 meter Fastie Ebert spectrometer with reciprocal line dispersion of 3 Å/mm. A background image with blocked pump is subtracted from each frame and the image at each delay is normalized to the fluctuations of the seed at 392 nm far from the emission lines of $N_2{}^+$. The spectra are normalized to the seed, which has two benefits. First it mitigates the impact of noise due to the laser fluctuations. Second, it reduces the temporal and spatial variations of the seed propagating in a medium with time-dependent index of refraction [18,19]. Spectral calibration is assured by comparing each spectrum with that of a nitrogen calibration spectral lamp.

The spectrum of $N_2{}^+$ emission $\mathbf{X}(\nu = 0) \leftarrow \mathbf{B}(\nu = 0)$ is recorded at each delay increment, and integrated for one second, which is orders of magnitude longer than the lifetime of the emission. This results in a series of spectra where each spectrum is a vertical stripe of pixels in Figs. 1(b) and 1(c) as a function of delay. Some selected rotational energy levels are shown on the Fig. 1(a). The collinear pump and probe are focused through a nitrogen cell at 760 Torr.

The spectrum at each delay is a vertical strip of the image. The integration time of the spectral recordings is one second, hence orders of magnitude longer than the lifetime of the emission. The temporal resolution in these measurements is solely due to the precision in determining the time delay between the center of the pump and probe ultrashort pulses. It should be noted that no emission is observed in the absence of seed pulse, which implies that the radiation is associated with a gain mechanism rather than a spontaneous emission or fluorescence. This confirms also that there is not enough spectral broadening of the 795 nm pump to create self-seeding.

Each horizontal line in Fig. 1(b) shows the time evolution of the emission as a function of pump-seed delay for individual P_J or R_J transition, with J being the rotational quantum number of the upper state. All the emissions undergo a strong intensity modulation at times corresponding to a multiple of half-revivals of $N_2{}^+$. The exact contribution of **B** and **X** wave packet in the observed modulation in time will be discussed in the Fourier transform analysis (Fig. 4).

Each rotational line is modulated with a period much smaller than the revival period. This fast modulation (visibly increasing with J in the **R** branch) is due to stimulated Raman emission that couples a state J to rotational states spaced by $|\Delta J| = 2$ [Fig. 1(b)]. The amplification of the seed persists for longer delays even in a cell at atmospheric pressure, when faster oscillations are not visible [Fig. 1(c)]. The strong modulation at revivals seen as dark and bright vertical lines are recorded for delays up to 150 ps (limited by the range of the translation stage) [Fig. 1(c)].

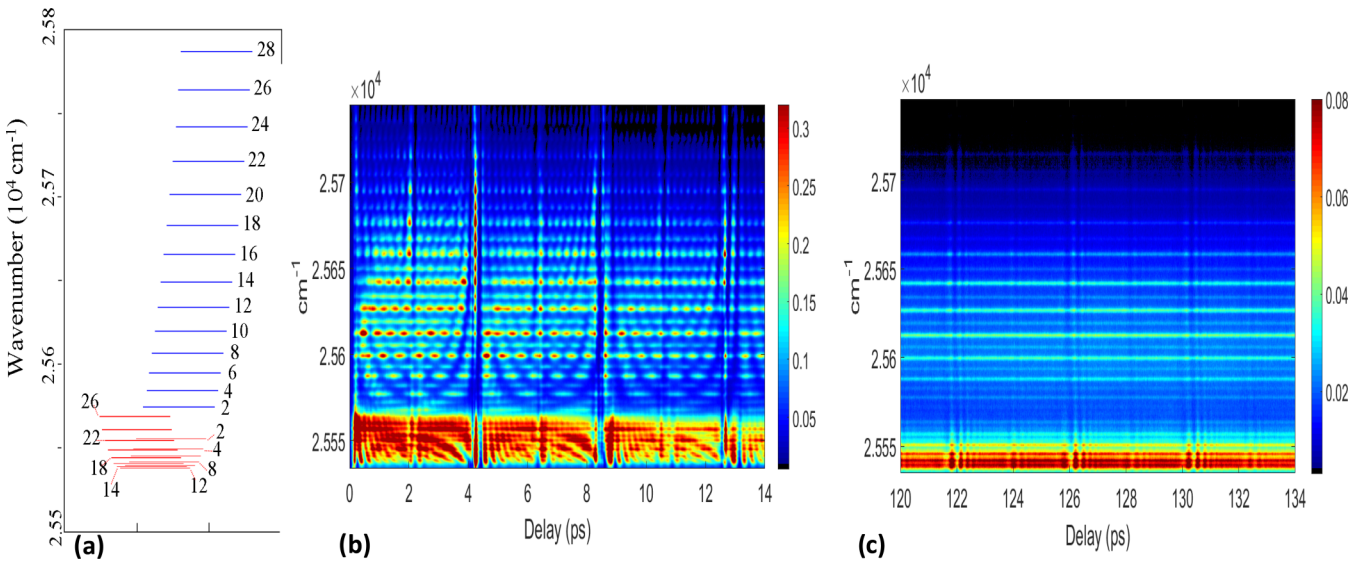

FIG. 1. (a) Energy diagram of the P branch (in red) and the R branch (in blue). The wave numbers are indicated on the left scale in cm^{-1}. The lines are calculated from reference [14]. The transitions are labeled by the rotational quantum number of the upper state. (b) The seed undergoes amplification on narrow lines corresponding to the rotational transitions $\mathbf{X}(v=0) \leftarrow \mathbf{B}(v=0)$ as a function of pump-seed delay. The time-dependent gain is visible as a function of delay between pump at 795 nm (940 μJ) and seed at 400 nm (40 nJ) for pure nitrogen at 760 Torr. The color coding shows the intensity increasing from blue to red. The signal strength is plotted in logarithmic scale as $\log_{10}[1+(y-y_{\min})/(y_{\max}-y_{\min})]$ in which $y_{\max}/y_{\min}$ is the highest/lowest pixel in all frames of the scan. Each individual rotational transition exhibits two time-dependent modulations. The oscillations are almost in phase for all transitions at times corresponding to multiples of half-revivals. Each rotational line undergoes oscillation with a shorter period that increases with the rotational number. Note that the emissions in **P** and **R** branches are not in phase. This can be seen by looking at the change of brightness on a vertical line. (c) The amplification of the seed persists for delays up to 150 ps in a cell at atmospheric pressure with a lower gain. At longer delays the fast modulation on transitions is not visible, only modulation at revivals is visible.

III. ANALYSIS AND DISCUSSION

It is a common practice to present the time-dependent gain by integration over groups of transitions, mainly because of limitation in resolving power of the spectrometer [21]. Our spectral resolution enables us to distinguish the rotational emission lines of the **R** branch, and some in the **P** branch. The gain integrated over all transitions of the **R** branch (red) and **P** branch (blue) is displayed in Fig. 2(a). Such a presentation provides physical insight into the dynamics of seed amplification. A steep rise of the gain is visible as the seed follows the pump laser. The exponential decays are fitted to both **P** and **R** emissions [black lines in Fig. 2(a)] as a function of seed delays from zero to 45 ps. Both signals decay to $1/e$ of their maximum after 30 ps for nitrogen at 760 Torr (100 ps for nitrogen at 100 Torr).

Both **P** and **R** emissions are modulated at revivals and fractional revivals with the oscillation period increasing at larger time delays and the modulation depth decreasing. The oscillations of the integrated **P** and **R** emissions are not quite in phase as shown in the inset of Fig. 2(a).

While one would be tempted to associate the exponential decay seen in Fig. 2(a) with a decay of population inversion [21], the fact that gain is observed up to 150 ps delay contradicts this interpretation. The gain at R_{12} in Fig. 1(c) is 2% of its value compared to average gain at delays in Fig. 1(b). One might speculate that decoherence is driven by random local fields due to the plasma environment in which the molecules—neutral and ionized—move and collide. The optically driven cation dipoles responsible for emission experience dephasing due to collisions and randomly varying environmental field. The former are modeled by a phase relaxation time T_2, and the latter by a cross relaxation time T_3, a situation well known for dyes in solution [22].

Figures 2(b) and 2(c) show the time-dependent emission from individually selected rotational lines (labeled by the rotational number of the upper state) as a function of seed delay from the same pump and seed intensity interacting with a nitrogen cell at 100 Torr. The highest rotational lines visible in the **R** branch are selected in Fig. 2(b).

A collective emission followed by absorption of the cation molecules, triggered by the seed, is observed at half-revival. This coherence driven gain has been referred to as superradiance [23] in recent papers [6,9]. The in-phase emission from the adjacent **R** lines only lasts for 400 fs. The fast oscillation period decreases with rotational number. This oscillation, as can be seen in Fig. 1(b), is no longer visible after the gain drops to $1/e$ of its maximum [Fig. 1(c)], which suggests that the coherence enhanced gain is lost after a certain delay. The gain at each rovibrational transition depends on the phase of states involved in the stimulated emission. The probability of emission is proportional to the dipole moment $\langle \Psi_{J,B}|\mu.e|\Psi_{J-1,X}\rangle$, which, for an **R** transition from upper state J, has a time-dependent phase of $2\pi c\{[B_B J(J+1) - B_X J(J-1)]\}t$. If we assume that the ionizing pulse sets

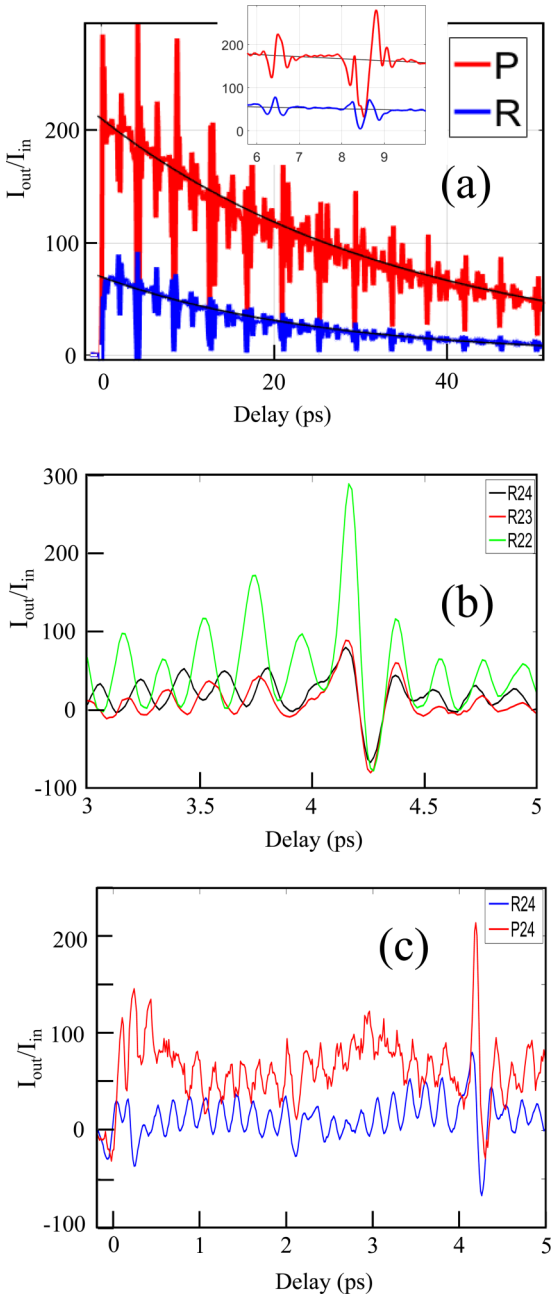

FIG. 2. (a) Gain in **P** (top) and **R** (bottom) emission integrated over transitions from **B** to **X** with $\Delta J = -1$ and $\Delta J = +1$ versus delay between pump and seed. This is another representation of the measurements of Fig. 1. Inset (a): time evolution from 6–10 ps showing oscillations visible in the **P** and **R** branch, out of phase with different frequency components. (b) Gain evolution for **R** transitions from states $J = 22$ (green/gray), 23 (red/dark gray), and 24 (black/black). (c) Emission for R_{24} (lower curve) and P_{24} (upper) from the same upper state. Vertical axis: ratio of integrated spectrum at time t with respect to that in the absence of pump beam. The spectral integration domain is chosen for each graph, according to a particular region of interest [in (a) over the **P** and **R** branch and in (b) and (c) only the area under the individual line transition is considered].

the time zero for the rotational states, each state evolves based on its rotational constant and angular momentum. The emission stimulated by the seed undergoes maxima and minima based on the relative phases of the connecting states.

The emission from individual lines at the high energy is presented in [Fig. 2(b)], in which both gain and absorption are realized. Our measurements suggest that the relative phase between the rotational states has a major role in the amplification of the seed, dominating any possible contribution from population inversion. The nearest Raman transitions impart a population modulation upon each state J proportional to $\alpha \exp[2i\pi c B_\ell (J+2)(J+3)t] + \beta \exp[2i\pi c B_\ell (J-2)(J-1)t]$, where α and β are probabilities of Raman transitions for $\Delta J = 2$ and $\Delta J = -2$, respectively. The oscillation frequency on each rotational transitions is increasing with the rotational state number J as shown in Fig. 2(b).

At delays corresponding to fractional revivals both absorption and emission are observed (e.g., at a half-revival, the emission is enhanced at 4.2 ps and the absorption is recorded at 4.32 ps). For other time delays, the emission from rotational lines is modulated over a zero floor and no absorption is recorded. The observation of absorption on individual emission lines suggests the possibility of coherent population trapping, in which the wave packet no longer interacts with light. In this case any population in the upper state can make transitions to the state orthogonal to the trapped one [24]. Absorption or gain will be observed depending on the phase of the rovibrational states.

Comparing the seed amplification from a common upper state **B** reveals the importance of dynamics in the ground state **X**. In Fig. 2(c), the two transitions from upper state $J = 24$ to lower state $J = 23$ and $J = 25$ result in two distinct lines of $\mathbf{R_{24}}$ and $\mathbf{P_{24}}$, respectively. It can be seen that at delays outside of the revival times, the two lines are 180 degree out of phase, a phase opposition that we attribute to the stimulated Raman. When the population is transferred by stimulated Raman from $J = 23$ to $J = 25$ in the **X** state, the transition probability of the $\mathbf{R}_{24}$ line is enhanced at the expense of lowering the transition probability of the $\mathbf{P}_{24}$. The nearly perfect out-of-phase relation in the emissions observed from the same upper state suggests that the gain is enhanced by transient inversion due to the phase relation between the states. Both lines experience synchronized emission and absorption at times corresponding to alignment and antialignment. The in-phase emission is not perfect for all rotational states as is visually observed by following the brightness of a vertical line in Fig. 1(b). This suggests a role of stimulated Raman in shifting the wave-packet population in favor of $\Delta J = 1$ or $\Delta J = -1$. The Fourier analysis of individual emission lines had been discussed in the literature [10,11]. In this work we are more interested in the time picture and the phase relation of these emissions.

In order to gain a better understanding of the time dynamics of the emission, we made a simulation using the time-dependent Schrödinger equation. In our model two electronic levels of N_2^+ were considered: $\mathbf{X}(\nu = 0)$ and $\mathbf{B}(\nu = 0)$ with a dipole transition independent of the rotational states. Rotational states were uniformly populated at time zero from $J = 0$ to $J = 20$, with their phases set to zero. The populations were set to $P(\mathbf{X}) = 0.7$ and $P(\mathbf{B}) = 0.3$. A seed pulse with an intensity of 4×10^{10} W/cm^2 and a duration of 24 fs caused

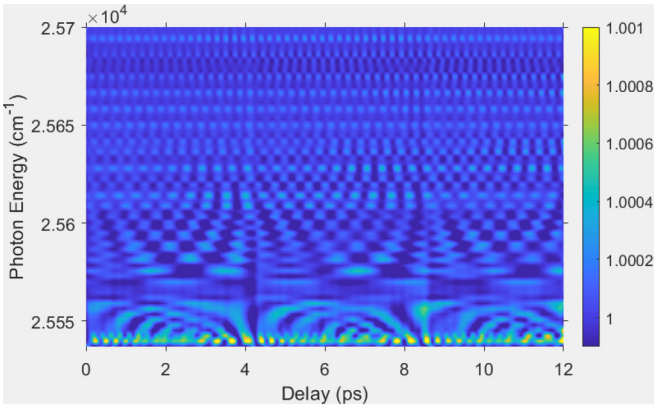

FIG. 3. Simulation of the time-dependent gain defined as $I_{\text{out}}/I_{\text{in}} = \exp\{-2kL\mathcal{I}m[\chi(\omega)]\}$ where k is the wave vector, and L the length of the medium. The $\mathbf{X}(v=0)$ and $\mathbf{B}(v=0)$ states were considered, with $J=0$ to $J=20$. The states are dipole coupled by a probe pulse centered at 391 nm that mixes populations. The emission is calculated from the induced polarization of the system over a period of 12 ps. The P branch modulation is not clear due to Moiré effects.

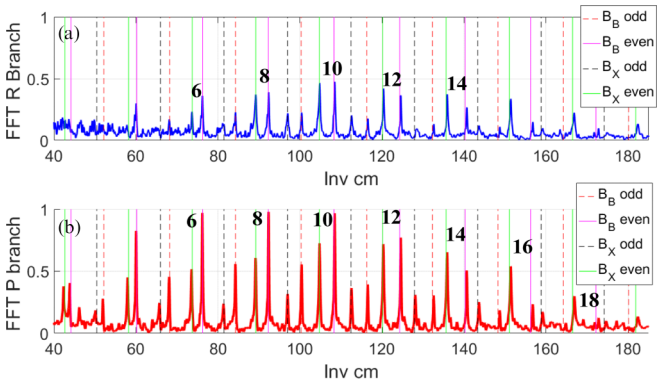

FIG. 4. The Fourier amplitude of **R** (top) and **P** (bottom) branch emissions. The horizontal axis is the frequency in the unit of cm^{-1}. The Fourier transform is plotted on a grid defined by Raman transitions of $\Delta J = -2$ in **B** and **X** states. The distribution of **X** is shifted to higher rotational states for both cases. The **R** branch connects to lower states of **X** as compared to **P**. This result is in agreement with exchange of orbital angular momentum to higher (**P**) and lower (**R**) values.

electric dipole coupling between the states and redistributed the population, depending on the relative phases of the states.

The total dipole moment of the system versus time was calculated for 12 ps, from which the linear susceptibility $\chi(\omega)$ of the medium in the frequency domain was calculated. The gain or loss of the seed spectrum was calculated from the imaginary part of the susceptibility (Fig. 3).

The simulation resembles the experimental observation of time-dependent gain at each individual transition. The parabolic structure of spectrum-delay graph replicates the experimental observation in Fig. 1(b). The phase delay between emission lines is also captured in the simulation by following the brightness in a vertical line of the figure. The simulation shows the modulation of the gain with stimulated Raman process driven by the seed pulse. Since the simulation is based on unimolecular interaction with light, the collective effect of in-phase emission at revivals is not observed.

A qualitative representation of the rotational wave-packet distribution is obtained through a Fourier transform of the emission lines in both **P** and **R** sections of the spectrum. The absolute values of the Fourier transforms of the integrated emission from the two branches are presented in Fig. 4 for the nitrogen cell at 100 Torr. The Fourier transform of the **P** (red/bottom) and **R** (blue/top) branches are presented separately in two plots with vertical grid lines corresponding to the Raman transitions of $\Delta J = -2$ in the **B** and **X** branch. Dashed lines correspond to the upper states with odd rotational numbers and solid lines correspond to the even states.

The Fourier transform of the emission is well aligned with the grid of the Raman transitions from cations. The spin statistics of nitrogen leads to having the population ratio of two to one between even and odd states of the thermal sample, which does not hold for the stimulated emission [25]. The Fourier transform reveals the signature of the wave packet in both **B** and **X** states, with a distinct shift in distribution. The distribution is shifted to the higher rotational states in the ground state as compared to the excited state. This can be visualized by comparing the Fourier transform component of adjacent rotational lines in **B** and **X**. For transitions from lower rotational numbers the amplitude of **B** is higher than **X**. This trend is reversed for rotational states higher than 10 in the **R** branch and higher than 12 in the **P** branch. For example, the ratio of **B** to **X** contribution at rotational number 6 in the **R** branch is 3/2, while at rotational number 14 the same ratio is 2/3 in the **R** branch emission. The shift in distribution had been explored by Azarm *et al.* [25] by comparing stimulated and spontaneous emission.

The shift in the wave-packet distribution in **B** and **X** states suggests that the two states have different interaction with ultrashort pulses. Both distributions are shifted to higher rotational numbers than a thermal distribution [26], with **X** state occupying the highest rotational numbers. By comparing the Fourier amplitude of **B** and **X** in lower rotational states one might conclude that the **B** state has a higher population that the **X** state, hence the stimulated emission would be governed by a traditional population inversion. Gain is observed for all the rotational states contributing in the observed Raman process of Fig. 4, independently of the ratio of **B**/**X**. We conclude therefore that the gain is not determined by the population inversion but by the coherence in the system. This coherence has been referred to as lasing without inversion [27,28]. This gain could be further tailored by engineering the wave packet in the system with a two pulse alignment [29] or a chirped seed counteracting the chirp in the level spacing of the rotational levels.

IV. CONCLUSION

We have performed high-resolution spectroscopy of N_2^+ emission $\mathbf{X}(v=0) \leftarrow \mathbf{B}(v=0)$ in a pump-seed setup, using ultrashort pulses. By careful measurements of the time-dependent emission from well-identified rotational lines, we observe the coherence involved in obtaining gain from ni-

trogen molecular ions created by ultrashort high-energy laser pulses. Our study suggests that the transition between high gain and low gain, in pump-seed studies, could be due to a loss of coherence in the system. This loss of coherence can be due either to collisions, or to the varying field evolution as the electrons and ions evolve towards a steady-state plasma [30]. The gain survives for up to 150 ps (even at atmospheric pressure), when the phase relation between individual emissions is lost. Resonant stimulated Raman scattering is responsible for the transients of the gain in the medium. When the phase of the levels is preserved this gain is further enhanced by coherence in the system. This effect is further enhanced at times corresponding to the rotational revival of the molecules, in which various rotational states are in phase. Our study suggests that coherent control of the rotational states in the molecular ion may result in control of the brightness of such emissions.

ACKNOWLEDGMENTS

We have benefited from long discussions with Paul Corkum, Michael Spanner, Mathew Britton, and Patrick Laferriere from NRC and the University of Ottawa. This work is supported by the US Department of Energy (DOE) (DE-SC0011446), and the Army Research Office (ARO) (W911-NF-1110297).

[1] A. Braun, G. Korn, X. Liu, D. Du, J. Squier, and G. Mourou, Self-channeling of high-peak-power femtosecond laser pulses in air, Opt. Lett. **20**, 73 (1995).

[2] X. M. Zhao, P. Rambo, and J. Diels, Filamentation of femtosecond UV pulses in air, in *Quantum Electronics and Laser Science Conference*, edited by T. Heinz, G. Stegeman, J. Bokor, and R. Slusher, Vol. 16 of OSA Technical Digest (Optical Society of America, Baltimore, 1995), paper QThD2.

[3] Q. Luo, W. Liu, and S. L. Chin, Lasing action in air induced by ultra-fast laser filamentation, Appl. Phys. B **76**, 337 (2003).

[4] Y. Liu, P. Ding, G. Lambert, A. Houard, V. Tikhonchuk, and A. Mysyrowics, Recollision-Induced Superradiance of Ionized Nitrogen Molecules, Phys. Rev. Lett. **115**, 133203 (2015).

[5] J. Yao, S. Jiang, W. Chu, B. Zeng, C. Wu, R. Lu, Z. Li, H. Xie, G. Li, C. Yu, Z. Wang, H. Jiang, Q. Gong, and Y. Cheng, Population Redistribution Among Multiple Electronic States of Molecular Nitrogen Ions in Strong Fields, Phys. Rev. Lett. **116**, 143007 (2016).

[6] G. Li, C. Jing, B. Zeng, H. Xie, J. Yao, W. Chu, J. Ni, H. Zhang, H. Xu, Y. Cheng, and Z. Xu, Signature of superradiance from a nitrogen-gas plasma channel produced by strong-field ionization, Phys. Rev. A **89**, 033833 (2014).

[7] M. Richter, F. Morales, M. Spanner, O. Smirnova, and M. Ivanov, Optical lasing during filamentation in the nitrogen molecular ion: ro-vibrational inversion, in *Electro-Optics, 2017*, pages CG–P–15, Munich, Germany (Optical Society of America, Baltimore, 2017).

[8] M. Matthews, F. Morales, A. Patas, A. Lindinger, J. Gateau, J. Kasparian, N. Berti, S. Hermelin, M. Richter, T. Bredtmann, O. Smirnova, J.-P. Wolf, and M. Ivanov, Amplification of intense light fields by nearly free electrons, Nat. Phys. **14**, 695 (2018).

[9] M. Lei, C. Wu, A. Zhang, Q. Gong, and H. Jiang, Population inversion in the rotational levels of the superradiant N_2^+ pumped by femtosecond laser pulses, Opt. Exp. **25**, 4535 (2017).

[10] B. Zeng, W. Chu, G. Li, J. Yao, H. Zhang, J. Ni, C. Jing, H. Xie, and Y. Cheng, Real-time observation of dynamics in rotational molecular wave packets by use of air-laser spectroscopy, Phys. Rev. A **89**, 042508 (2014).

[11] H. Xie, B. Zeng, G. Li, W. Chu, H. Zhang, C. Jing, J. Yao, J. Ni, Z. Wang, Z. Li, and Y. Cheng, Coupling of N_2^+ + rotational states in an air laser from tunnel-ionized nitrogen molecules, Phys. Rev. A **90**, 042504 (2014).

[12] Z. Liu, J. Yao, J. Chen, B. Xu, W. Chu, and Y. Cheng, Near-Resonant Raman Amplification in the Rotational Quantum Wavepackets of Nitrogen Molecular ions Generated by Strong Field Ionization, Phys. Rev. Lett. **120**, 083205 (2018).

[13] R. F. Wuerker, S. Schmitz, T. Fukuchi, and P. Straus, Lifetime measurements of the excited states of N_2 and N_2^+ by laser-induced fluorescence, Chem. Phys. Lett. **150**, 443 (1988).

[14] L. Klynning and P. Pages, The band spectrum of N_2^+, Phys. Scr. **25**, 543 (1982).

[15] H. Stapelfeldt and T. Seideman, Colloquium: Aligning molecules with strong laser pulses, Rev. Mod. Phys. **75**, 543 (2003).

[16] S. Varma, Y.-H. Chen, and H. M. Milchberg, Quantum molecular lensing of femtosecond laser optical/plasma filaments, Phys. Plasmas **16**, 056702 (2009).

[17] J. A. Yeazell and C. R. Stroud, Jr., Observation of fractional revivals in the evolution of a Rydberg atomic wave packet, Phys. Rev. A **43**, 5153 (1991).

[18] C. Marceau, S. Ramakrishna, S. Génier, T.-J. Wang, Y. Chen, F. Théberge, M. Châteauneuf, J. Dubois, T. Seideman, and S. L. Chin, Femtosecond filament induced birefringence in argon and in air: Ultrafast refractive index change, Opt. Commun. **283**, 2732 (2010).

[19] F. Calegari, C. Vozzi, S. Gasilov, E. Benedetti, G. Sansone, M. Nisoli, S. De Silvestri, and S. Stagira, Rotational Raman Effects in the Wake of Optical Filamentation, Phys. Rev. Lett. **100**, 123006 (2008).

[20] V. P. Kandidov, V. Yu. Fedorov, O. V. Tverskoi, O. G. Kosareva, and S. L. Chin, Intensity clamping in the filament of femtosecond laser radiation, Kvant. Electron. **41**, 382 (2011).

[21] H. Zhang, C. Jing, J. Yao, G. Li, B. Zeng, W. Chu, J. Ni, H. Xie, H. Xu, S. L. Chin, K. Yamanouchi, Y. Cheng, and Z. Xu, Rotational Coherence Encoded in an "Air-Laser" Spectrum of Nitrogen Molecular Ions in an Intense Laser Field, Phys. Rev. X **3**, 041009 (2013).

[22] D. W. Vahey and A. Yariv, Effects of spectral cross relaxation and collisional dephasing on the absorption of light by organic dye molecules, Phys. Rev. A **10**, 1578 (1974).

[23] R. H. Dicke, Coherence in spontaneous radiation processes, Phys. Rev. **93**, 99 (1954).

[24] O. A. Kocharovskaya and Y. I. Khanin, Amplification and lasing without inversion, Phys. Rep. **219**, 175 (1992).

[25] A. Azarm, P. Corkum, and P. Polynkin, Optical gain in rotationally excited nitrogen molecular ions, Phys. Rev. A **96**, 051401(R) (2017).

[26] L. Arissian, B. Kamer, and A. Rasoulof, Effect of rotational wave packets on the stimulated emission of nitrogen with light filament, Opt. Commun. **369**, 215 (2016).

[27] O. A. Kocharovskaya and Y. I. Khanin, Electric events synchronized with laser filaments in thunderclouds, Sov. Phys. JETP **63**, 945 (1986).

[28] M. O. Scully, S. Y. Zhu, and A. Gavrielides, Degenerate Quantum-Beat Laser: Lasing without Inversion and Inversion Without Lasing, Phys. Rev. Lett. **62**, 2813 (1989).

[29] K. F. Lee, I. V. Litvinyuk, P. W. Dooley, M. Spanner, D. M. Villeneuve, and P. B. Corkum, Two-pulse alignment of molecules, J. Phys. B **37**, L43 (2004).

[30] D. A. Romanov and R. J. Levis, Postionization medium evolution in a laser filament: A uniquely nonplasma response, Phys. Rev. E **86**, 046408 (2012).